Traffic Sign Orientation Estimation from Images Using Deep Learning

Raluca-Diana Chiş[1][a], Mihai-Adrian Loghin[1][b], Cristina Mierlă[1][c],
Horea-Bogdan Mureşan[1][d] and Octav-Cristian Florescu[2]
[1]*Department of Computer Science, Babeş-Bolyai University, Cluj-Napoca, Romania*
[2]*Grab, Geo Engineering, Vision, Cluj-Napoca, Romania*
{*raluca.chis, mihai.loghin, cristina.mierla, horea.muresan*}*@ubbcluj.ro, octav.florescu@grab.com*

Keywords: Yaw Estimation, Traffic Signs, Deep Learning.

Abstract: This study presents our findings on estimating the horizontal rotation angle (yaw) of traffic signs from 2D images using deep learning techniques. The aim is to introduce novel approaches for accurately estimating a traffic sign's orientation, with applications in automatic map generation. The primary goal is to associate a traffic sign with a road correctly. The main challenge consists of both attempting to estimate the left/right orientation of a sign from 2D images and accurately estimating the rotation of the sign in degrees. Our approach involves the usage of a classifier for determining the orientation of a traffic sign in relation to the observer. Furthermore, we tried to transfer the weights obtained from classification to regression models and study the impact on performance. Our best results are obtaining an L1 loss as low as 10.34° for yaw estimation and an accuracy equal to 62% for orientation class assessment. The image data was obtained from Grab's Kartaview platform and was split into training/validation/testing while accounting for traffic sign class and shape balancing.

1 INTRODUCTION

The main motivation behind our research is the need to map traffic signs with their related roads correctly. According to Adewopo et al. (Adewopo et al., 2023), T-intersections and four-way intersections are the places with some of the highest traffic accident rates and these are also the places with a high conglomeration of traffic signs, which can easily be misinterpreted. Our context is the following: Grab creates accurate maps, with the main focus on (but not restricted to) the region of Southeast Asia, which are then integrated into their application. One focus use case of the applications is to offer GPS-navigation for deliverers, thus driver's safety and efficiency in traffic are strongly related to the accuracy of the provided maps. As such, GrabMaps is properly updated with the latest changes in terms of traffic rules. Thousands of images are collected from roads daily and any new traffic signs are automatically detected.

In order to map a sign to a road, it is necessary to know towards which road it is oriented (Figure 1). The purpose of our research is to facilitate the software that is able to compute the rotation angle (yaw) of a traffic sign from a single 2-dimensional image. This angle will be calculated as the yaw rotation relative to the heading of the camera that captured the image. This research topic is particularly difficult since in many cases even the human eye is unable to determine to which road a traffic sign is addressed.

Taking into consideration the state-of-the-art classification and regression models on angle and pose estimation, the following pre-trained models have been applied: WideResNet (Zagoruyko and Komodakis, 2016), ResNext (Xie et al., 2016), Swin (Liu et al., 2021). The results of the three models do not differ greatly, although certain particularities for each model were observed. Experiments were conducted with a set of 1617 images of traffic signs (provided by Grab), manually annotated by us with orientation classes (**LEFT**, **RIGHT** and **CENTER**) and with rotation angles. One of our best results is a mean absolute error equal to 10.34° for yaw estimation with the Swin Transformer model. Moreover, a 62% accuracy was obtained for the assessment of the orientation class with the ResNext model.

Regarding the structure of the paper, Section 2 presents the work of other researchers on yaw esti-

[a] https://orcid.org/0009-0000-0445-3961
[b] https://orcid.org/0000-0001-6112-6713
[c] https://orcid.org/0000-0002-2777-1353
[d] https://orcid.org/0000-0003-4777-7821

Chiş, R.-D., Loghin, M.-A., Mierlă, C., Mureşan, H. B. and Florescu, O.-C.
Traffic Sign Orientation Estimation from Images Using Deep Learning.
DOI: 10.5220/0013115900003890
Paper published under CC license (CC BY-NC-ND 4.0)
In *Proceedings of the 17th International Conference on Agents and Artificial Intelligence (ICAART 2025) - Volume 3*, pages 233-240
ISBN: 978-989-758-737-5; ISSN: 2184-433X
Proceedings Copyright © 2025 by SCITEPRESS – Science and Technology Publications, Lda.

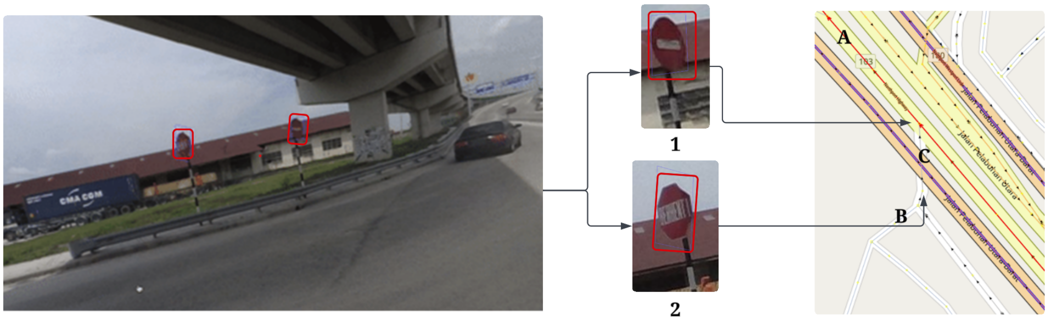

Figure 1: Visual explanation of the problem: users provide images from roads, traffic signs are identified, each sign is mapped to a road according to its yaw rotation. In this case, sign **1** is mapped to road **A**, sign **2** to road **B** and **C** is the approximate location of the picture.

mation. Section 3 describes the pre-processing techniques applied to the dataset and our approach to the proposed problem. Further, Section 4 presents the performance of our experiments in comparison with existing works. In the end, Section 5 summarizes our findings and presents ideas for future improvements.

2 RELATED WORK

The detection of a sign and the identification of a bounding box for it are crucial before orientation estimation. Approaches exist in 2D ((Hara et al., 2017), (Raza et al., 2018)) or 3D ((Prisacariu et al., 2010), (Kendall et al., 2015), (Mousavian et al., 2017)). Research in orientation evaluation focuses on classification and regression. Kanezaki et al. (Kanezaki et al., 2018), Raza et al. (Raza et al., 2018), and Salas et al. (Rodriguez Salas et al., 2021) propose the use of convolutional neural networks for classification. In (Kanezaki et al., 2018) an unsupervised model was developed, called ”RotationNet”, that takes as input multiple images with different perspectives on an object and returns the object category and pose. In (Rodriguez Salas et al., 2021), the angle of rotation on the Z-axis from a two-dimensional image is estimated, using images from MNIST (Deng, 2012), rotated with an angle between [0, 2π]. The angle values range from -180° to 180° and were sampled in 16 classes. (Raza et al., 2018) propose a CNN model to detect pedestrian orientation using head pose and full-body images. They achieved an accuracy of 0.91 for head pose detection and 0.92 for full-body orientation.

In terms of using a regression-based approach, Kendall et al. (Kendall et al., 2015) present a CNN-based model, that uses transfer learning from GoogLeNet (Szegedy et al., 2014) model. Another relevant study that uses deep convolutional neural networks is described in (Hara et al., 2017), with the best architecture based on the ResNet-101 model and pretrained weights. The results show a Mean Absolute Error (MAE) value of 12.6° for the EPFL Multi-view Car Dataset (Ozuysal et al., 2009) and 30.2° for the TUD Multi-view Pedestrian Dataset (Andriluka et al., 2010). Okorn et al. (Okorn et al., 2022) describe a self-supervised method, which estimates the relative position of an object between neighboring objects with Modified Rodrigues Projective Averaging.

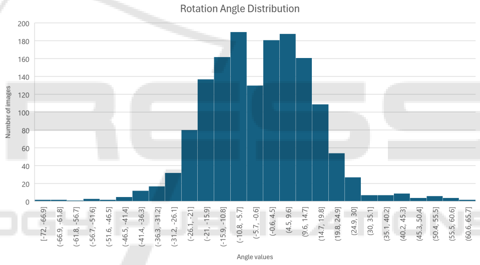

Figure 2: Distribution of the yaw angle values.

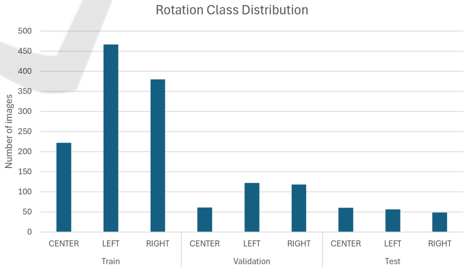

Figure 3: Distribution of the rotation classes.

A particularly interesting approach to the problem is using several consecutive images of the same sign. The SuperGlue (Sarlin et al., 2020) model proposes an attentional graph neural network for matching the key-points of two input images, thus enabling cross-image communication. Similarly to PoseNet, the study from (Cui et al., 2019) revolves around the use of image pairs, whose features are extracted with the SIFT and SURF algorithms, shifted and matched correspondingly. An objective function is created for integrating these features in the 3D coordinate system, which leads to the estimation of the traffic sign plane.

There are several approaches addressing the problem of orientation estimation. Although some researchers employ multiple views of an object to estimate its pose (Okorn et al., 2022), (Kanezaki et al., 2018), a more practical and accessible method involves using a single image of the object, as we propose in the following section. With a novel dataset and stronger deep learning models, we provide an original contribution to the state of the art of orientation estimation.

3 METHODOLOGY

3.1 Dataset

The dataset used for provided by Grab, a major player in the automatic mapping industry, containing images of traffic signs in Detroit, U.S.A. The dataset includes 223619 images with varying degrees of quality, each containing at least a traffic sign. There are 42 different traffic sign types, ranging from **TURN_RESTRICTION_U_TURN_LEFT_US** to **SPEED_LIMIT_35_US**. The dataset also contains the bounding box of each sign in a rectangular shape, revealing the approximate dimensions of the sign. Due to the presence of multiple traffic signs and significant background noise, the images underwent cropping before initiating the training pipeline. The best results were obtained using square images with varying sizes, depending on the dimensions of the traffic sign.

The process of manually annotating images initially included two rotation orientation classes (**LEFT** and **RIGHT**) along with angle estimation. Upon further review, an additional rotation class was introduced to the dataset, categorizing front-facing images into a new group called **CENTER**. This group encompasses images with rotation angles ranging between -5° and 5°, which are mostly imperceptible to the human eye. This range was established empirically, based on observations from analyzing more images with low rotation angles and the results from explainability models for them.

The study aimed to compile a set of images exhibiting a wide range of rotation angles, spanning from front-facing orientations to extreme rotations. Based on this criterion, a subset of the images was selected. Still, a significant percentage (78.47%) of the signs have a rotation angle between -30° and 30° (Fig. 2). However, the models struggle to categorize signs with angles within this range due to small differences in position. The quality of the images was also a crucial criterion, as different individuals took pictures in traffic while driving and using non-professional cameras. Each image was manually verified to reduce the likelihood of noisy inputs. The set contains 1534 records, with 26 traffic sign types and four categories: square-shaped, wide rectangle, tall rectangle and suspended rectangle. For experiments, the partitioning of training, test, and validation sets was carried out considering the distribution of rotation orientation categories and sign types. Figure 3 displays the rotation class distribution over the three image sets. 1069 images were selected for training, 301 for validation and 164 for testing.

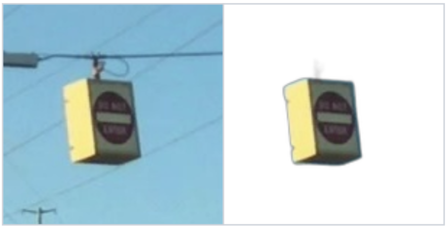
(a) Original (b) No background

Figure 4: Example of background bias, caused by the mismatch between the rotation of the power cable and of the traffic sign.

Another relevant study direction was background noise reduction. To achieve that, experiments were performed with background-free images. To remove the background, the python library BackgroundRemover [1] has been employed, which uses a state-of-the-art model, hierarchical U-Net (Qin et al., 2020). Removing backgrounds highlighted the importance of image context and potential bias. An illustrative example is shown in Figure 4. The left image (a) shows a power cord suggesting central rotation, while the sign itself appears rotated to the left. In contrast, the image on the right (b) shows the traffic sign isolated from the background, thus eliminating potential confusion caused by the power cable.

3.2 Models

To tackle the challenge, models have been sought out that are effective for both regression and classification tasks. These models were then subjected to the procedure shown in Fig. 5. Considering the approaches from the related literature, we have observed the use of models based on ResNet-50 (Koguciuk et al., 2021) and also the use of convolutional neural networks as the prime way to solve the problem (Kendall et al., 2015). We also aimed to study

[1] https://pypi.org/project/backgroundremover/

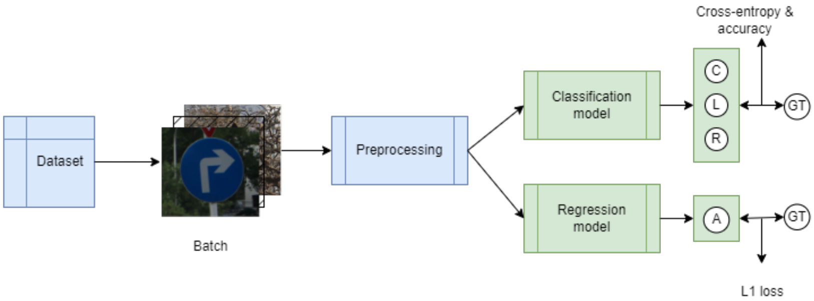

Figure 5: Diagram representing the process of sending the data through the classification (upper part) and regression models (lower part), with the respective loss functions at the end. *C*, *L* and *R* stand for Center, Left and Right, respectively; *A* stands for the angle predicted in terms of rotation degrees; *GT* stands for ground truth.

the impact of the model type and architecture on the obtained results. Thus, we decided to use three main models as the base of the research: WideResNet (wide_resnet101_2) (Zagoruyko and Komodakis, 2016), ResNext (resnext101_32x8d) (Xie et al., 2016) and Swin (swin_s) (Liu et al., 2021).

Swin Transformer was chosen as it is architecturally different from the other models that were used, which contributed in the active learning process that was used to obtain the regression data set. With this diversity of the models in place, the process of verifying the quality of the labelled data became much easier.

The models were implemented using PyTorch, with initial weights from IMAGENET1K_V2, for WideResNet and ResNext, and IMAGENET1K_V1, for Swin. The weights were chosen based on the best results from the available benchmarks for models. Our approach was based on transfer learning, the most important part was to choose the most optimal values for the base model and its options for training.

3.3 Quality Metrics

Given that we are approaching the problem from two perspectives for pose estimation, classification and regression, several metrics have been implemented to evaluate our results. The metrics presented in this section have been selected after multiple tests and considering the problem definition.

For the regression task we only considered the L1 loss function, known as mean absolute error (MAE) (Hodson, 2022), to measure the results. This decision was made since we needed an exact estimate as to how far the model's results were from the ground truth in terms of degrees. As for the classification problem, we utilised the categorical cross entropy (CCE) loss function (Rusiecki, 2019; Wang et al., 2022), accuracy, precision, recall and f1-score to train and evaluate the models.

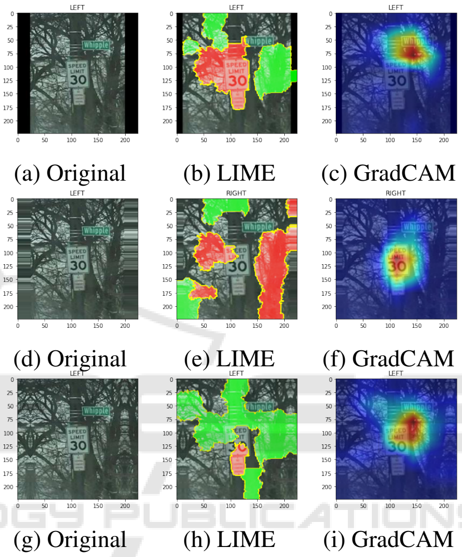

(a) Original (b) LIME (c) GradCAM

(d) Original (e) LIME (f) GradCAM

(g) Original (h) LIME (i) GradCAM

Figure 6: LIME and GradCAM explanations given an image with class left and several image augmentations. The expectation is that a model will focus on the sign and its edges. (a, b, c) show the results after constant padding, (d, e, f) for edge padding, and (g, h, i) for reflection padding.

3.4 Explainability

To gain a better understanding of our results, we also employed the use of two interpretation options for the models. The decision was based on the fact that large neural network models often present a black-box decision-making process. As such, it is important to understand why or if we should trust the decision-making done by the models (Molnar, 2022; Selvaraju et al., 2017; Ribeiro et al., 2016).

For both the regression and classification problems presented in the previous sections, we have generated explanations using LIME. This technique is based on creating several interpretable models, such as decision trees, and feeding them with variations of the input data to gain an understanding of the importance of each feature (Molnar, 2022; Ribeiro et al., 2016). The explanations are presented in the form of a mask with positive (green) and negative (red) impact areas on the image for the given prediction (Molnar, 2022).

To gain an even better understanding, we also employed the use of another model-agnostic technique known as GradCAM which was implemented specifically for classification problems using neural networks. It brings several advantages since it offers model-specific deterministic explanations. This technique is used by attaching the GradCAM explainer to one of the layers of the model and only depending on the layer it is attached to will the explanation change. The resulting explanation appears in the form of a heatmap over the input image showcasing the most important area for the given prediction (Selvaraju et al., 2017).

4 RESULTS

4.1 Classification Results

After analyzing the dataset, it was noticed that around 250 images could not be clearly characterized as left or right. Those records were represented by signs that were photographed front-facing the camera. In order to organize the samples of the dataset into distinct classes we manually extracted and annotated the images as a new class, **CENTER**. This addition was relevant to the rotation class because it allows each of the 3 classes to be more specialized in an angle rotation interval. A rough estimation for the rotation class **CENTER** interval is [-5, 5] degrees of rotation. This improvement helped the model understand better that a rotation angle closer to 0 leads to a front-facing sign, while a rotation angle further away from 0 may indicate one of the **LEFT** or **RIGHT** classes.

Several experiments have been conducted before concluding that the best results would be for images cropped directly in a square format, with and without background (the notations ”bg” will be used for images with background, and ”no bg” for images without background). After analyzing the models using the previously mentioned explainers, it was noticed that the models sometimes are misled by power lines or other objects belonging to the background. With this information, we believed that a model trained on images without background has the capabilities to better focus on the sign and its rotation, rather than the background. The experiments were mainly run for the classification part of the problem, which simplifies the overall problem as previously stated. Some of the results for different forms of image padding can be observed in Fig. 6. The final experiments were done on square images, specifically cropped this way from the source image.

The Cross-entropy loss was used to evaluate the models during training and the corresponding results are displayed in Table 1. Optimizers Adam and Stochastic Gradient Descent (SGD) have been used alternatively with a learning rate (LR) equal to 3e-5, which was set experimentally. The learning rate scheduler from PyTroch *StepLR* has been applied with a gamma factor equal to 0.1 and a step size of 7, implying that the LR has been decayed by a factor of 0.1 every 7 epochs. All models have been trained for 100 epochs, although the results are consistent after only 20 epochs. Regarding the sizes of the experiment sets, they are constant (whether or not the images have a background): the train set has 1069 images, the validation one 301 and the test set 164 images. The optimal found batch size was 4.

4.2 Regression Results

For the regression problem, we have only considered experiments on images with and without background. In our first experiments, we considered that the most extreme scenarios could help us better understand the model's capabilities. The motivation for running experiments on datasets with or without background is similar to the one mentioned before, keeping the same interpretations. As seen in Figure 7 the most accurate results were obtained for a model trained on images with background, but this was only the case for some situations. Over multiple experiments, it has been noticed that the no background model focuses better on the sign. Another good aspect of the no background model is that it does not give mainly negative numbers for the results.

The optimizers, learning rate and scheduling use the same hyperparameters as before. The loss function for the values presented in Table 2 is L1 (MAE) loss. The models have been trained for 40 epochs, as it was noticed that at this point the results stabilize. The datasets used have the same size, with the mention that the notations for the y-angle values were used and the optimal batch size was 16.

4.3 Discussion

Before discussing the results, it is important to note that the results in Tables 1 and 2 were the best overall results based on the best parameters found for each model. The models were evaluated continuously throughout the research as we corrected and completed the dataset based on an active learning

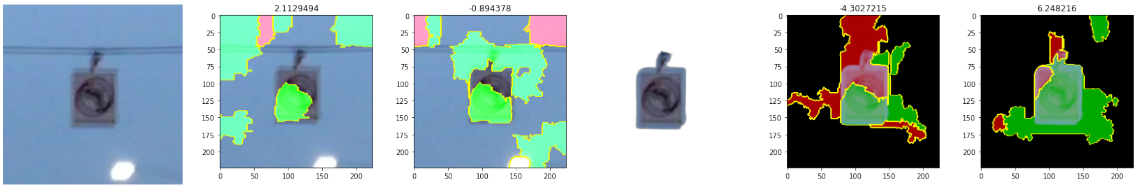

(a) Original (b) Background model (c) No background model (d) Original (e) Background model (f) No background model

Figure 7: LIME results for an image considered in the centre class, with and without background, having a 3° ground truth rotation. The results in (b, e) are for a model only trained on images with background and the results in (c, f) are for a model only trained on images without background.

Table 1: Experimental results for all three classification models under different optimizers and image inputs (bg - images with full background; no bg - images that were processed and had their background removed, CE - Cross-entropy).

Model	Optm.	Image input	Tr. Loss	Val. Loss	Test Loss	Tr. Acc	Val. Acc	Test Acc	Test Prec.	Test Recall	Test F1
WideResNet	SGD	bg	1.01	1.00	1.05	0.51	0.52	0.48	0.48	0.48	0.48
	SGD	no bg	1.06	1.31	1.05	0.43	0.47	0.43	0.43	0.43	0.43
	ADAM	bg	2.59	1.43	1.66	0.46	0.45	0.43	0.43	0.43	0.43
	ADAM	no bg	0.89	1.04	1.34	0.58	0.52	0.40	0.38	0.38	0.38
ResNext	SGD	bg	1.03	1.04	1.03	0.48	0.44	0.48	0.48	0.48	0.48
	SGD	no bg	1.02	49.72	1.03	0.48	0.48	0.48	0.48	0.48	0.48
	ADAM	bg	**0.14**	**0.95**	1.11	**0.99**	**0.63**	0.56	0.56	0.56	0.56
	ADAM	no bg	0.95	1.42	**0.90**	0.91	0.60	**0.62**	**0.62**	**0.62**	**0.62**
Swin	SGD	bg	1.01	1.02	1.16	0.48	0.47	0.32	0.32	0.32	0.32
	SGD	no bg	1.01	1.02	1.13	0.46	0.45	0.35	0.35	0.35	0.35
	ADAM	bg	0.19	1.97	1.50	0.93	0.46	0.40	0.42	0.42	0.42
	ADAM	no bg	0.55	1.53	1.12	0.76	0.46	0.43	0.43	0.43	0.43

Table 2: Experimental results for all three regression models under different optimizers and image inputs (bg - images with full background; no bg - images that their background removed).

Model	Optimizer	Image input	Train Loss	Val. Loss	Test Loss
WideResNet	SGD	bg	13.59	12.91	10.35
	SGD	no bg	13.6	12.94	10.50
	ADAM	bg	**6.93**	11.85	11.00
	ADAM	no bg	9.49	11.65	10.59
ResNext	SGD	bg	13.61	13.83	10.40
	SGD	no bg	13.60	13.55	10.39
	ADAM	bg	7.25	12.05	11.26
	ADAM	no bg	9.38	11.90	11.76
Swin	SGD	bg	13.55	12.91	**10.34**
	SGD	no bg	13.50	12.80	10.37
	ADAM	bg	10.10	13.66	11.12
	ADAM	no bg	11.01	**11.60**	11.64

approach. Throughout this process, the model with the best results changed continuously as more diverse data was added. In the end, all the models obtained similar results, indicating that the problem's solution is related directly to the quality of the data.

For the classification task, the most common best performances were on the set of no-background images using the ADAM optimizer, with the best performance being given by the model ResNext as in Table 1. Most of the time the models ended up overfitting easily on the training data set, obtaining results as good as 0.99 at most, but the validation results staggered at around 0.57 at most. The same drop in accuracy can also be seen in the test data for most of the models. The drop in accuracy might be due to the difference in class balance between the subsets of data. The type of the sign in the image did not affect the performance of our models.

On the regression task, a similar situation can be noticed by comparing the results in Table 2 and Fig. 7. This time WideResNet had the best performance on training data and Swin for test data, but as before the results were not that far apart between the models. It might seem counter-intuitive that this time the results on the test data are better than that for the other splits in some cases. This can be explained by the distribution of the angle values in the dataset and how they were further distributed between the subsets.

In addition to the numerical results, we also obtained visual explanations via LIME and GradCAM. In Fig. 6 we can see the explanations for the classification task using both approaches and in Fig. 7 the explanations for the regression task only using LIME, since GradCAM is classification-specific. Based on the obtained explanations, we can conclude that the models have successfully learned to identify objects of interest for class and angle prediction, which background information confuses the model, and that background removal is a useful tool for encouraging this learned behavior.

Compared to other articles, the prediction of the rotation class in terms of accuracy and loss might be considered satisfactory. In (Rodriguez Salas et al., 2021) the lowest error rate was equal to 0.93%, which is higher than our smallest, 0.9%. Considering that our best accuracy is 62% on test data, 63% on validation data and 99% on training data, we could say that it is worse than 91% from (Raza et al., 2018) or 81.17% presented in (Kanezaki et al., 2018). We consider two reasons for this: the difficulty of working with traffic signs for this task and the usage of the CENTER class. Working with images depicting objects with increased depth (such as humans in (Raza et al., 2018) or cars, beds, mugs and so on in (Kanezaki et al., 2018)), provides the benefit of having more particular and easily categorizable sides of an object. Traffic signs, on the other hand, tend to be quite thin, and their left perspective does not differ much visually from the right one.

The CENTER class represents a bridge between the two other classes, and these images are harder to classify due to their poorer representation in the dataset. Of all images, only 22.35% belong to the CENTER class. Moreover, in the train set 20.76% of the images are centered and in the test set 36.58%, which caused the CENTER category to have a greater influence on the final results, although the models were less trained for it. Our best model obtained on the test set for the RIGHT category an accuracy of 73%, followed by the LEFT class with 61% and CENTER with 34%. If we neglect the CENTER class, the final accuracy would be 67%.

In terms of angle prediction, our degree of error is much lower than that of multiple other research papers. As in the previous paragraph, the comparison might not be as direct, given the usage of different datasets, but it is still relevant to understanding the true quality of the results. Given that the lowest error in our case is equal to 10.34° on the test, with a 6.93° error on the train data, we are within the expected error rate, even below it. We are below the results of articles such as (Cui et al., 2019), where the authors obtained a mean error of 14.45°, but above those of article (Okorn et al., 2022). It is worth mentioning that in (Okorn et al., 2022) the authors note a higher error for images with more noise in them, something that was addressed in this paper by using background removal to eliminate the noise created by background information. A smaller error rate was also obtained in comparison with (Hara et al., 2017), where the MAE value for the EPFL Multi-view Car Dataset (Ozuysal et al., 2009) is 12.6° and for the TUD Multi-view Pedestrian Dataset (Andriluka et al., 2010) it is equal to 30.2°.

5 CONCLUSION AND FUTURE WORK

Our work stands out from the others by using performing deep/transfer learning methods and a manually annotated dataset. Our models have obtained an MAE score as low as 10.34° and an accuracy of up to 62% on unseen data. Using the explainable models, *LIME* and *GradCAM*, provided a deeper understanding of the learning process and of the challenges faced. Up to this point, conclusions have been derived by separating the problem into regression and classification.

A main focus point in our research is the impact of background information/noise on the angle and rotation class prediction tasks. The experiments, at first glance, have shown that removing the background information does not yield better or worse results, but using explanation methods, we can determine that it helps the models focus on the object of interest significantly more. Based on the results from the images with and without background, it can be seen that the background noise does not affect the models' performance most of the time. The results, as evaluated in comparison, tend not to have a strong deviation from each other.

Some problems that were highlighted using the *LIME* and *GradCAM* tools require further experimentation and testing. Similarly, the impact of padding, removing, or expanding the background for signs must be explored in more depth, as it may lead to better results for both classification and regression. Currently, we could only determine that it is much more favorable to crop based on a square box around the sign.

For further experiments, we plan on expanding the problem solution with the use of a multitask model. The model would supposedly have two heads: one for classification and one for regression. Given the results of the two heads, we plan to calculate the final results as previously mentioned. Most of the problem will come down to how the loss function is computed.

ACKNOWLEDGMENT

This research has been funded by Grab, as part of a collaboration with Babeş-Bolyai University. All data used are the property of Grab, who provided access for the authors to their data set through their Kartaview platform of images captured with onboard cameras on US roads.

REFERENCES

Adewopo, V., Elsayed, N., ElSayed, Z., Ozer, M., Wangia-Anderson, V., and Abdelgawad, A. (2023). Ai on the road: A comprehensive analysis of traffic accidents and autonomous accident detection system in smart cities. In *2023 IEEE 35th International Conference on Tools with Artificial Intelligence (ICTAI)*, pages 501–506.

Andriluka, M., Roth, S., and Schiele, B. (2010). Monocular 3d pose estimation and tracking by detection. In *2010 IEEE Computer Society Conference on Computer Vision and Pattern Recognition*, pages 623–630.

Cui, Z., Liu, Y., and Ren, F. (2019). Homography-based traffic sign localization and pose estimation from image sequence. *IET Image Processing*, 13.

Deng, L. (2012). The mnist database of handwritten digit images for machine learning research. *IEEE Signal Processing Magazine*, 29(6):141–142.

Hara, K., Vemulapalli, R., and Chellappa, R. (2017). Designing deep convolutional neural networks for continuous object orientation estimation.

Hodson, T. O. (2022). Root-mean-square error (rmse) or mean absolute error (mae): when to use them or not. *Geoscientific Model Development*, 15(14):5481–5487.

Kanezaki, A., Matsushita, Y., and Nishida, Y. (2018). Rotationnet: Joint object categorization and pose estimation using multiviews from unsupervised viewpoints. In *Proceedings of the IEEE Conference on Computer Vision and Pattern Recognition (CVPR)*.

Kendall, A., Grimes, M., and Cipolla, R. (2015). Posenet: A convolutional network for real-time 6-dof camera relocalization. *CoRR*, abs/1505.07427.

Koguciuk, D., Arani, E., and Zonooz, B. (2021). Perceptual loss for robust unsupervised homography estimation. In *Proceedings of the IEEE/CVF Conference on Computer Vision and Pattern Recognition (CVPR) Workshops*, pages 4274–4283.

Liu, Z., Lin, Y., Cao, Y., Hu, H., Wei, Y., Zhang, Z., Lin, S., and Guo, B. (2021). Swin transformer: Hierarchical vision transformer using shifted windows. *CoRR*, abs/2103.14030.

Molnar, C. (2022). *Interpretable Machine Learning*. Leanpub, 2 edition.

Mousavian, A., Anguelov, D., Flynn, J., and Kosecka, J. (2017). 3d bounding box estimation using deep learning and geometry.

Okorn, B., Pan, C., Hebert, M., and Held, D. (2022). Deep projective rotation estimation through relative supervision.

Ozuysal, M., Lepetit, V., and Fua, P. (2009). Pose estimation for category specific multiview object localization. In *2009 IEEE Conference on Computer Vision and Pattern Recognition*, pages 778–785.

Prisacariu, V. A., Timofte, R., Zimmermann, K., Reid, I., and Van Gool, L. (2010). Integrating object detection with 3d tracking towards a better driver assistance system. In *2010 20th International Conference on Pattern Recognition*, pages 3344–3347.

Qin, X., Zhang, Z., Huang, C., Dehghan, M., Zaiane, O. R., and Jagersand, M. (2020). U2-net: Going deeper with nested u-structure for salient object detection. *Pattern Recognition*, 106:107404.

Raza, M., Rehman, S.-U., Wang, P., and Peng, B. (2018). Appearance based pedestrians' head pose and body orientation estimation using deep learning. *Neurocomputing*, 272:647–659.

Ribeiro, M. T., Singh, S., and Guestrin, C. (2016). "why should i trust you?": Explaining the predictions of any classifier. In *Proceedings of the 22nd ACM SIGKDD International Conference on Knowledge Discovery and Data Mining*, pages 1135–1144, New York, NY, USA. Association for Computing Machinery.

Rodriguez Salas, R., Dokladal, P., and Dokladalova, E. (2021). A minimal model for classification of rotated objects with prediction of the angle of rotation. *Journal of Visual Communication and Image Representation*, 75:103054.

Rusiecki, A. (2019). Trimmed categorical cross-entropy for deep learning with label noise. *Electronics Letters*, 55.

Sarlin, P.-E., DeTone, D., Malisiewicz, T., and Rabinovich, A. (2020). Superglue: Learning feature matching with graph neural networks.

Selvaraju, R. R., Cogswell, M., Das, A., Vedantam, R., Parikh, D., and Batra, D. (2017). Grad-cam: Visual explanations from deep networks via gradient-based localization. In *2017 IEEE International Conference on Computer Vision (ICCV)*, pages 618–626.

Szegedy, C., Liu, W., Jia, Y., Sermanet, P., Reed, S., Anguelov, D., Erhan, D., Vanhoucke, V., and Rabinovich, A. (2014). Going deeper with convolutions.

Wang, Q., Ma, Y., Zhao, K., and Tian, Y. (2022). A comprehensive survey of loss functions in machine learning. *Annals of Data Science*, 9(2):187–212.

Xie, S., Girshick, R. B., Dollár, P., Tu, Z., and He, K. (2016). Aggregated residual transformations for deep neural networks. *CoRR*, abs/1611.05431.

Zagoruyko, S. and Komodakis, N. (2016). Wide residual networks. *CoRR*, abs/1605.07146.